Intra-tumoral epigenetic heterogeneity and aberrant molecular clocks in hepatocellular carcinoma

Paula Restrepo[1,2,3,4+], Adrian Bubie[1+], Amanda J. Craig[5], Daniel Cameron[6], Ismail Labgaa[7], Myron Schwartz[8], Swan Thung[9], Gustavo A. Stolovitzky*[10,11], Bojan Losic*[1,12], Augusto Villanueva*[5,13]

[+] *These authors contributed equally to this study.*

[1]*Departments of Genetics and Genomic Sciences, Icahn School of Medicine at Mount Sinai, New York, NY, 10029*

[2]*Graduate School of Biomedical Sciences, Icahn School of Medicine at Mount Sinai, New York, NY 10029, USA*

[3]*Black Family Stem Cell Institute, Institute for Regenerative Medicine, Icahn School of Medicine at Mount Sinai, New York, NY 10029, USA*

[4]*Kimberly and Eric J. Waldman Department of Dermatology, Icahn School of Medicine at Mount Sinai, New York, NY 10029, USA*

[5]*Division of Liver Diseases, Department of Medicine, Tisch Cancer Institute, Icahn School of Medicine at Mount Sinai, New York, NY, 10029*

[6]*Applied Bioinformatics Laboratories, NYU Grossman School of Medicine, New York, New York*

[7]*Department of Visceral Surgery, Lausanne University Hospital CHUV (Switzerland).*

[8]*Department of Surgery, Icahn School of Medicine at Mount Sinai, New York (US).*

[9]*Department of Pathology, Icahn School of Medicine at Mount Sinai, New York (US).*

[10]*Department of Pathology, NYU Grossman School of Medicine, New York, New York*

[11]*Biomedical Data Sciences Hub, NYU Langone Health, New York, New York*

[12]*Genomics and Enterprise AI, Ambry Genetics, Aliso Viejo, California*

[13]*Division of Gastroenterology and Hepatology, Perlmutter Cancer Center, NYU Grossman School of Medicine, New York, New York*

***Address for correspondence:**

***Gustavo A. Stolovitzky, PhD**
Department of Pathology
NYU Grossman School of Medicine
Biomedical Data Sciences Hub
NYU Langone Health
gustavo.stolovitzky@nyulangone.org

***Bojan Losic, PhD**
Department of Genetics and Genomic Sciences
Tisch Cancer Institute, Cancer Immunology
Diabetes, Obesity and Metabolism Institute
Icahn Institute for Data Science and Genomic Technology
Icahn School of Medicine at Mount Sinai, New York, NY 10029
bojan.losic@mssm.edu; blosic@ambrygen.com

***Augusto Villanueva, MD, PhD**
Perlmutter Cancer Center, NYU Grossman School of Medicine
Smilow Research Center
522 First Avenue, Smilow Building, 7th Floor, Suite 704, New York, NY 10016
augusto.villanueva@nyulangone.org

ABSTRACT

There is limited understanding of the epigenetic drivers of tumor evolution in hepatocellular carcinoma (HCC). Here we characterize the epigenetic contribution of methylation to intra-tumoral heterogeneity (mITH) using regional enhanced reduced-representation bisulfite sequencing DNA methylation data from 47 early stage, treatment-naive HCC biopsies across 9 patients by quantifying regional differential methylation across promoters and CpG islands, while overlapping with methylation age markers. Furthermore, we integrate these data with matching RNA-sequencing, targeted DNA sequencing, tumor-infiltrating lymphocyte (TIL), and hepatitis-B viral expression data. We found substantial mITH signatures in promoter and enhancer sites across 44% of patients in our cohort that highlight a novel axis of ITH that is not otherwise detectable from RNA analysis alone. Additionally, we identify an epigenetic tumoral aging measure that reflects a complex tumor fitness phenotype as a potential proxy for tumor clonality. Associating clinical outcomes with epigenetic tumoral age using 450k array data from 377 patients with HCC in the TCGA-LIHC single-biopsy cohort we found evidence implying that epigenetically old tumors have lower fitness yet higher TIL burden. Our data reveal a novel, unique epigenetic axis of ITH in HCC that merits further exploration.

INTRODUCTION

Hepatocellular carcinoma (HCC) is a common yet lethal form of liver cancer that has one of the fastest growing incidence rates globally,[1,2] typically arising in patients with a background of chronic liver disease, such as hepatitis B or C (HBV or HCV) infection, alcohol use disorder, and metabolic dysfunction associated steatotic liver disease (MASLD). Despite recent improvements in systemic therapies, drug resistance remains a challenge and median survival in advanced stages is still less than two years. We and others have shown significant molecular intra-tumoral heterogeneity (ITH) in 30-40% of HCC.[3-5] This includes complex mixtures of subclonal cancer populations evolving over time and interacting with non-tumoral stromal and immune cells in the microenvironment,[6] a key molecular feature underlying drug resistance in HCC.

Previous studies of ITH in HCC have leveraged experimental designs with multi-regional sampling from the same tumor.[3,4,6-8] These studies found that driver mutations in genes such as *TERT* promoter, *TP53*, and *CTNNB1* tend to be founder events present in all regions of the tumor, and increased ITH correlates with worse prognosis and clinical outcomes in patients with HCC.[3,4,7,8] Our previous work found distinct ITH-dependent patterns of spatio-temporal interactions between HCC and immune cells along with strong evidence of spatially heterogeneous immunoediting in multi-regional samples,[3] indicating that HCC ITH cannot be fully characterized through mutation data alone.[3,4]

One notable yet relatively underexplored aspect of ITH in HCC is the role of DNA methylation. Previous examination of epigenetic drivers highlight promoter hypermethylation of tumor suppressor genes as an important mechanism for tumorigenesis and disease progression in HCC and some of its background etiologies.[9,10] We detected aberrant methylation patterns in HCC that can be distilled into signatures predictive of patient prognosis and survival, indicating a potentially

useful avenue for biomarker discovery.[9] A previous study examining DNA methylation using multi-regional sampling in a small cohort of HCCs reported significant epigenetic heterogeneity among tumors, in contrast to strong interindividual homogeneity of nonmalignant liver tissue.[4]

A key aspect of methylation data is its ability to predict molecular epigenetic age, which measures proxies of biological age of a tissue as opposed to its chronological age.[11] These "epigenetic clocks" have been extensively validated in normal tissue and used to examine the biological aging process and its relation to human diseases, including cancer.[11-13] However, the role of methylation age in ITH has not been well characterized in HCC to date.

To further investigate the unique contributions of DNA methylation to HCC evolution and ITH, here we use enhanced reduced representation bisulfite sequencing (eRRBS) to obtain methylation profiles from multiregional biopsies of 9 previously analyzed patients.[3] By adding another layer of methylation data to existing molecular ITH profiles, we explicitly compare ITH signatures derived from RNA expression and DNA methylation data and find key differences. We leverage well-known associations between conserved methylation signatures and chronological patient age to derive estimates of differentially aging tumoral regions that reflect novel aspects of tumor evolution and heterogeneity not captured by expression profiling alone.[11,12] Integrating the TCGA-LIHC (HCC) cohort with our data, we find a differential tumoral aging profile that strongly associates epigenetically younger TCGA-LIHC tumors with greater DNA clonal diversity, tumor mutation burden (TMB), tumor fitness (poorer patient prognosis), and lower tumor infiltrating lymphocyte (TIL) burden. The differential regional aging of tumors is a novel axis of epigenetic ITH which may reflect a complex tumor fitness phenotype, serving as a useful proxy for tumoral evolution and ultimately the prognostic stratification of patients.

119 **RESULTS**

120

121 Spatial tumor methylation profiling via multi-regional sampling

122 We performed enhanced reduced representation bisulfite sequencing (eRRBS)[14] on 47 samples
123 from 9 HCC patients, including tumor (35 samples, including a technical replicate) and adjacent
124 non-tumoral regions (12 samples, **Fig 1A**). On average, we analyzed a median of 5 samples per
125 patient. All patients were treatment-naive at the time of the surgical resection. Most patients were
126 male (67%) with a median age of 61 years, median tumor size of 6.5 cm, and about 55% (5/9)
127 had hepatitis B infection as the most common underlying liver disease (**Fig 1B**). Drawing on
128 previously reported data for these samples,[3] tumor purity was determined using SNP-array data
129 via ASCAT (version 2.4) and histological examination.

130 Since eRRBS data offers a granular view of methylation status at specific CpG sites both within
131 and outside of promoter regions, we designed our regional methylation analysis to take advantage
132 of both promoter-specific and site-specific sensitivity. We performed a site-specific analysis
133 considering only well-covered CpG sites regardless of proximity to a transcriptional start site
134 (TSS). We then aggregated sites within some proximal region of a TSS and conducted essentially
135 a gene-wise promoter-based analysis allowing a reasonable comparison to both 450k methylation
136 array data (and methylation aging signatures derived from it) and bulk RNA-seq transcriptional
137 profiling (**Fig. 1C**).

138

139 Regional epigenetic ITH (mITH) reveals novel differential methylation associations

140 Using the normalized site-specific methylation data, we performed a PCA analysis to quantify the
141 leading axes of variation driving patient and regional specific DNA methylation signatures (**Fig.**
142 **2A**). The first two principal components collectively explain 26% of the total variance, but the
143 leading principal component separates tumor from adjacent normal samples and broadly stratifies
144 tumors by degree of tumor-infiltrating-lymphocyte (TIL) burden (defined by VDJ read burden

145 normalized for library size from RNAseq) (Spearman rho = 0.76, P < 2.2e-16) and number of VDJ
146 clones (Spearman rho = 0.82, P < 2.2e-12) (**Fig 2C**). While there is strong evidence of patient-
147 specific clustering, there are also outlier regions which demonstrate that the relative scale of ITH
148 can overwhelm patient-specific variance, as demonstrated by the second principal component
149 which reveals that patient 8 is a strong outlier (**Fig 2A**), and these conclusions are maintained
150 using the promoter-specific methylation data as well (**Supp Fig 1A**).
151 To directly derive multi-regional signatures reflecting epigenetic ITH (mITH) across patients'
152 tumors, we carried out within-patient differential methylation analyses at both the site (**Fig 2B,**
153 **Supp Table 1**) and the promoter level (**Fig 3A, Supp Table 3**). Patients 2, 3, and 10 displayed
154 significant mITH (**Fig 2B, Fig 3A**), while patient 4 revealed the highest ITH with region H4.c having
155 the highest relative number of differentially methylated promoters (1071 differentially methylated
156 (DM) promoters, FDR < 0.05). Patient 6, previously described as being heavily immune infiltrated
157 displayed only comparatively minor mITH DM at region H6.a (1 DM promoter, FDR < 0.05, **Fig**
158 **3A**) despite TCR sequencing showing extensive heterogeneity in TCR across the different tumor
159 regions.[3] Although patients with more biopsies sampled per tumor have more power to detect
160 mITH, the most densely sampled patient, P9 (n=6), had very few mITH DM sites or promoters, in
161 contrast to patient 3 with only 2 tumor sites sampled, yet detected more heterogeneity (**Fig 2B,**
162 **Fig 3A**). This suggests that our average sampling rate of 5 biopsies per tumor was sufficient to
163 capture the leading effect of mITH.
164 To compare regional mITH signatures with those associated with HBV viral expression, TIL
165 burden, and tumor vs adjacent normal, we leveraged our previously reported results using these
166 patients.[3] We identified site and promoter level mITH DM signatures driven by TIL, tissue type
167 (normal vs HCC tumor), and HBV viral expression (**Fig 2B, Supp Fig 1B, Supp Table 2 (sites),**
168 **Supp Table 4 (promoters)**). As expected, the HCC tumor-specific signature had the most DM
169 sites (FDR < 0.05, 184,504 Sites, **Fig 2B**) and promoters (FDR < 0.05, 5,458 promoters, **Supp**
170 **Fig 1B**), followed by TIL-related sites and promoters, with the HBV-driven signatures having the

171 fewest sites or promoters (**Fig 2B, Supp Fig 1B**). In all global DM signatures, there is a bias
172 towards hypomethylation (**Fig 2B, Supp Fig 1B**). We identified overlapping significant DM sites
173 among global and within patient regional mITH DM signatures to examine the contribution of
174 general cancer or immune specific methylation patterns to regional methylation gradients. We
175 observed unexpectedly little overlap in DM sites among global and regional comparisons (**Fig 2D**)
176 and among mITH DM profiles between patients. Instead DM overlaps came from global
177 comparisons, intra-patient overlaps, with also some individual patient regions overlapping with
178 global DM sites. This suggests that mITH DM profiles are not only unique on a per-patient basis
179 but may also be uniquely independent of general tumor- or immune-driven transcriptional
180 regulation programs.
181
182 <u>Enhancer overlap with differential methylation signatures</u>
183 We overlapped DM sites with known enhancer regions reported in the HACER database and
184 identified sites residing in putative promoter regions defined as within 2Kbp downstream or 1Kbp
185 upstream of a transcription start site (TSS). While most DM sites fall into promoter regions, sites
186 whose genomic coordinates overlap with a known enhancer region and a putative gene promoter
187 are termed 'dual-overlap', regions. We find an aberrant, global TIL-associated bias towards
188 hypermethylation in enhancers, and a less pronounced hypermethylation in dual-overlap sites
189 (**Supp Fig 2A)**. This hypermethylation bias in enhancers is preserved in intra-patient, regional-
190 relative mITH DM sites (**Supp Fig 2B**). Hypermethylation occurring at enhancers but not
191 promoters in samples with a bias for TIL may indicate the activation of TIL associated genes due
192 to promoter hypermethylation often silencing transcription while hypermethylation of enhancers
193 can also be activating. This phenomenon of immune infiltration associated with enhancer, not
194 promoter, DMR has been reported in squamous lung cancer,[15] and conversely with recurrent
195 enhancer hypomethylation associated with poor prognosis in HCC.[16]
196

197 mITH signature is not a simple recapitulation of transcriptomic profiling

198 Since ITH is a complex manifestation of cancer evolution, we combined DM promoters with
199 differentially expressed (DE) genes from RNAseq data to gain an integrative view of the data.[3]
200 DM promoters and DE genes had zero overlap for 32 out of 39 regional comparisons across 9
201 patients. A handful of regional comparisons, which belong to patients 2, 3, 4, and 5, had low
202 overlap relative to the DNA methylation (max = 34.06%, median = 17.07%) and to the RNA (max
203 = 10%, median = 1.590%) (**Fig 3B**). Sample sizes from gene overlap only allowed us to correlate
204 DNA methylation and gene expression log-fold changes in three contrasts, with no significant
205 correlation in two samples (H4.c and H4.a&c) and a moderate negative correlation in the third
206 (H3.a; Spearman rho = -0.409, P = 4.5 e-03) (**Fig 3B)**. Taken together with existing literature,[11,12]
207 these observations suggest that the mITH described by DM profiling offers a unique signal that
208 may not be captured by gene expression information alone.

209

210 Tumoral hyper-aging and inter-regional heterogeneity predicted by methylation clock

211 To quantify how mITH relates to tumor clonal evolution, we calculated the predicted methylation
212 age of the tissue across tumor samples and adjacent normal tissue using methylation clocks.[11]
213 While only 12 CpG sites of the 353 used to inform Horvath's model had reasonable coverage in
214 the RRBS sequencing data (**Fig 1C**), the promoter-aggregated site analysis provided coverage
215 overlap at the gene level of 240 of the 353 genes from the methylation clock mode (**Fig 1C**). This
216 allowed us to predict tissue methylation age across samples at the gene level.
217 To visualize how mITH might be driving downstream differences in clonal evolution, we compared
218 the relative tissue methylation age across tumor and normal for patients 2, 4, 8, 9 and 10, each
219 of which had three or more regionally sampled tumor sites and sampled adjacent normal tissue
220 (**Fig 4A**). While for all but patient 8 we found wide variance (variance ranges from 3.66e-03 to
221 1.34e-02 vs 5.63e-04 for patient 8) in the predicted methylation ages across regional samples
222 within tumor, the average relative tumoral methylation age was more advanced than the predicted

223 methylation age of the adjacent normal liver tissue for all patients. Tumoral relative hyper-aging
224 was greatest in patient 8, where average tumoral methylation age was 1.35 times greater than
225 that of the average predicted age of the adjacent liver tissue (**Fig 4B**), with a median tumoral
226 hyper-aging factor of 0.17x across patients. Tumor-normal blood relative methylation age ratios
227 calculated for two of three additional, previously reported, multi-regionally samples HCC patients
228 (GSE83691) validated this trend, though the remaining patient had a significant hyper-aging
229 signature of the adjacent normal tissue compared to the tumor (**Supp Fig. 3**).[4]
230 The ratio of predicted sample methylation ages to true patient age was used to determine a
231 relative tissue DNA methylation aging factor. This ratio was significantly positively correlated with
232 the second principal component of a promoter-aggregated site methylation PCA across regional
233 samples (**Fig 4C;** Spearman rho = 0.5, P = 0.002), with the tumoral samples from patient 8
234 demonstrating the largest hyper-aging effect compared to the true patient age. Predicted
235 methylation age ("Clock age") was also significantly correlated with PC2, but to a lesser degree
236 (**Fig 4C;** Spearman rho=0.31, P = 0.001). Neither measure correlated with other sample clinical
237 covariates. We also observed a negative correlation between predicted methylation clock age
238 and VDJ read burden (**Fig 4C;** Spearman rho = -0.36, P = 2.52e-04). These data indicate that
239 tumoral hyper-aging is a potentially useful quantitative proxy for mITH.
240
241 <u>Tumoral hyper-aging associates with reduced tumor clonality, decreased tumor fitness, and</u>
242 <u>"hotter", less clonal tumor microenvironment</u>
243 We applied our methylation-age prediction analysis to 366 single biopsy HCC samples from the
244 450k methylation array TCGA-LIHC cohort to validate our observation of tumor hyper-aging and
245 establish the association with patient survival and known clinical biomarkers for immune activity
246 such as TIL and tumor mutational burden (TMB). We observed advanced relative tumor
247 methylation-age in 260/366 (71%) HCC patients in the cohort, with an average methylation aging
248 factor of 1.22 and a median methylation aging factor of 1.15 (ratio of predicted tumoral methylation

249 age to patient diagnosis age; **Fig 5A**). Kaplan-Meier survival estimates were calculated for
250 patients organized by tumor methylation clock age into “old” and “young” groups, thresholded by
251 the median tumor aging factor (1.15). Patients with “old” methylation-aged tumors saw significant
252 survival benefit over patients with “young” tumors (HR=0.667, p=0.037; **Fig 5B**).
253 To investigate whether the relative tumor methylation age remains a significant predictor of patient
254 survival after regressing out known clinical covariates, we constructed a multivariable Cox
255 proportional hazard (cph) model using patient TMB, sex, tumor stage, and relative tumor age
256 factor (**Supp Table 5**). A regularized cubic spline was applied to the relative age factor to test for
257 non-linear effects on survival. We found relative tumor methylation age to have a significant
258 positive effect on patient survival (p=0.049) (**Supp Table 5**), with no evidence for a significant
259 non-linear effect. To demonstrate the improvement in survival prediction error using relative tumor
260 methylation age, we compared the time dependent integrated Brier scores for nested cph models
261 using the clinical covariates with and without the relative methylation age factor (**Fig 5C**).
262 Comparing the resulting prediction error curves under bootstrap resampling (see Methods) we
263 found that inclusion of relative methylation age factor reduces survival prediction error compared
264 to the model that does not include the measure (**Fig 5C, inset table**). Computing Brier scores
265 under cross-validation indicates these results are robust and will favorably generalize to other
266 datasets.
267 As we found advanced relative tumor DNA methylation age associated with improved patient
268 survival (decreased tumor fitness) in the TCGA, we investigated its association with other key
269 tumoral and immune molecular features. Performing VDJ-deconvolution of RNA sequencing data
270 from TCGA HCC samples matched with 450k array data,[17] we observed TIL burden and immune
271 clonality to be significantly higher amongst “old” relative tumor methylation age HCCs compared
272 to “young” tumors (p=0.016, p=0.046; **Fig 5D-E**), and PD-1 receptor expression typically
273 associated with T cell influx was similarly significantly upregulated in “old” tumors (p<0.01; **Fig**
274 **5F**). Interestingly, using the TCGA HCC DNA-sequencing data to determine and cluster somatic

275 mutations into clones, “old” HCCs were also found to have significantly fewer tumor clones
276 compared to “young” tumors ($p<0.01$; **Fig 5G**), and tended to have lower TMBs ($p=0.024$, **Fig**
277 **5H**). These results relate mITH by way of tumoral hyper-aging to reduced clonal complexity, hotter
278 and more clonal TIL burden, and decreased tumor fitness, in a much larger.

279 **DISCUSSION**

280

281 DNA methylation alterations in cancer are often difficult to systematically interpret outside of well-
282 studied examples such as promoter hypermethylation of tumor suppressor genes, hypo-
283 methylation of repeat-rich regions. This is true in part because of poor correlation to expression-
284 based characterizations of DNA-methylation changes. This translates into limited evidence on the
285 contribution of DNA methylation to ITH. In this work we provide the most comprehensive analysis
286 of epigenetic ITH in HCC reported to date. Using well-known epigenetic clocks, we show that
287 tumoral hyper-aging, which may be biologically related to a higher mitotic rate in tumor cells, is a
288 useful, novel metric for describing tumor evolution and mITH in both the multi-regional and single-
289 biopsy context. The chronological alteration of epigenetic profiles via progressive DNA
290 methylation has been extensively established in several normal tissues,[18] however its utility as a
291 proxy of mITH for malignancies has yet to be fully explored. From the point of view of multi-
292 regional sampling, we show that mITH effectively describes differential epigenetic aging for
293 spatially distal regions in HCC relative to the adjacent normal aging rate. In other words, different
294 parts of the same tumor are epigenetically aging at different rates, and on average these rates
295 are all higher than that of adjacent non-HCC liver tissue. Even from the point of view of single-
296 biopsy data such as the TCGA LIHC cohort, we show that, on average, even a single HCC biopsy
297 is older than the diagnosis age of the patient. In our previous work,[3] we established that a key
298 facet of ITH was immune-editing resulting from tumor-immune interactions which can effectively
299 constrain tumoral evolution.

300 Regional differential methylation underlying hyper-aging tends to implicate promoter regions, with
301 some overlapping enhancers, belonging to genes which are not differentially expressed in those
302 same regional comparisons reinforcing the importance of mITH in addition to transcriptomics.
303 Moreover, although some mITH sites were shared between individual patients' signatures and
304 global contrasts such as HCC status or TIL burden, there remains a high degree of patient

305 specificity in mITH patterning and an absence of significant inter-patient mITH site overlap. This
306 indicates highly specific epigenetic reprogramming between patients and can characterize tumor
307 evolution and behavior. Still, patients with marked mITH, such as patients 4 and 5, had strong
308 enrichment in DM signatures associated with TIL burden and HCC vs. adjacent normal liver. This
309 contrasts with patients with minimal mITH, such as patients 7 and 10, who were significantly
310 under-enriched in these contrasts. This underscores that mITH reflects an orthogonal axis of
311 tumoral evolution that is not well captured in a single biopsy context but can be captured in as
312 few as two biopsies (patient 3). This phenomenon of mITH and its effects on tumor clonal
313 evolution can be further assessed through the relative age of the tumor in regions with hyper-
314 aged, "old", tumors had reduced clonal burden and higher TIL burden. mITH also provides a rich
315 feature space from which to mine potential biomarkers of tumoral evolution and treatment
316 response in HCC. Given the relative granularity of eRRBS data compared to array-based DNA
317 methylation data, these spatial multi-regional mITH data add several previously uncharacterized
318 mITH-specific loci for potential downstream prioritization in other applications, including liquid
319 biopsies.
320 As of now, there are very few studies that evaluate mITH in cancer. A comprehensive
321 characterization of mITH in lung cancer found that ITH mapping to tumor suppressors was lower
322 than that of oncogenes. The authors suggested a greater selection pressure in these regions with
323 lower methylation ITH.[19] Another very recent publication in non-small cell lung cancer identified a
324 25-fold increase in interpatient heterogeneity in tumors as compared to normal samples, as well
325 as inter-patient methylation heterogeneity being greater than mITH.[20] In HCC, there have been
326 two studies using multiregional sampling and array-based DNA methylation to assess mITH.[4,8]
327 Unlike ours, the first study[4] did not include paired gene expression samples but confirmed
328 significant mITH with prognostic value. The second study, focused on driver events of HCC
329 evolution, detects higher levels of hypermethylation in curated epigenetic driver events at CpG
330 islands and promoter regions in addition to the detection of shared and distinct methylation

331 patterns.[8] Some limitations of our study include a relatively small sample size (despite being
332 among the largest HCC cohorts analyzed for mITH), limited external validation due to the lack of
333 publicly available multi-regional omics datasets, and the absence of a robustly trained epigenetic
334 clock specific for HCC.

335 This work has characterized an additional layer of molecular intra-tumoral heterogeneity, finding
336 that significant regional differential DNA methylation patterns in patient HCC tumors are unique
337 and poorly recapitulated in standard pooled or single-biopsy profiles. We also report on
338 accelerated epigenetic aging on a regional basis within tumors which serves as a novel proxy
339 measure for ITH. These data can provide new insights into mechanisms underlying ITH, as well
340 as a potential feature space for discovery of novel biomarkers.

341 **METHODS**

342

343 Sample collection

344 Patient recruitment and sample collection was performed as previously described.[3] Briefly,
345 patients were enrolled in the study at Icahn School of Medicine at Mount Sinai (ISMMS) and
346 provided informed consent for tissue biobanking. The study was approved by the Mount Sinai IRB
347 (IRB# HS-14-01011) and samples were provided by the ISMMS Tissue Biorepository (IRB# HS-
348 10-00135). All patients had early-stage hepatocellular carcinoma (HCC) per AASLD guidelines
349 and were treatment-naïve prior to surgical resection.[21] Frozen tissue samples from the same
350 tumor nodule were collected allowing for at least 1 cm of distance between each other. Samples
351 were selected from areas without macroscopic evidence of necrosis or hemorrhage.

352

353 RRBS sequencing and processing

354 DNA was extracted using the DNeasy blood and tissue kit (Qiagen) from 30mg tissue following
355 manufacturers protocol. RRBS sequencing was performed by the Epigenomics Core facility at
356 Weill Cornell Medical College using an in-house developed protocol consisting of restriction
357 enzyme digestion for enrichment of CpG sites, NGS library construction and bisulfite conversion
358 of cytosines.[14] 50bp single-read libraries were sequenced using the Illumina HiSeq 2500 platform
359 in high output mode.

360

361 Raw RRBS reads were trimmed using trim galore (v0.5.0) with the '-rrbs' flag enabled, and quality
362 control metrics were compiled using fastqc (v0.5.0). Reads were then aligned to the hg38 UCSC
363 reference genome using bismark (v0.22.3), bowtie2 (v2.4.1), and samtools (v1.11) with the
364 options to retain unmapped and ambiguously mapped reads enabled. A count matrix with
365 methylated and unmethylated counts for each sample was created using bismark's methylation
366 extractor tool (v0.22.3).

367

368 Differential methylation analysis

369 Differential methylation signatures were computed with edgeR following previously established
370 methodology outlined in Chen et al.[22] We used the generalized linear model framework in edgeR
371 because it allows for flexibility and robustness in analyzing complex experimental designs while
372 being able to account for technical and biological covariates. Briefly, this approach works by
373 adding extra columns to the design matrix to account for read coverage at each site or promoter,
374 therefore allowing for statistical analyses that mirror those typically used for RNA-seq.[22] This
375 analysis was performed in two settings: at individual CpG island sites (i.e. site-based), and at the
376 promoter level by aggregating counts falling within the same promoter regions (i.e. promoter-
377 based).

378

379 In the site-based analysis, sites with a minimum coverage of 10 reads across all samples were
380 retained. In the promoter-based analysis, counts for sites that fall within the same promoter region
381 were summed the nearestTSS function in the edgeR package.[22,23] These regions were defined
382 as within 2kb upstream or 1kb downstream of the nearest transcription start site annotation as
383 previously described.[22,23] Promoters with at least 10 aggregated reads across all samples were
384 retained for further analysis.

385

386 Site-based and promoter-based DM signatures were computed on a within-patient, regional-
387 relative basis, and on a global basis. In all analyses, sites, or promoters from mitochondrial, sex,
388 and unannotated chromosomes were removed from analysis. Total library size for all samples
389 was set as the sum of methylated and unmethylated counts. All dispersion estimates assumed
390 no mean-variance trend.

391

392 *Regional-relative DM signatures*

393 Within-patient regionally-relative DM signatures were computed using pooled sample
394 comparisons in an effort to directly sample epigenetic ITH while compensating for lack of
395 statistical power on a per-patient basis. Briefly, a generalized linear model using edgeR's RRBS
396 pipeline was created for each of the 39 within-patient comparisons across all 9 patients.[22] HBV
397 viral expression, measured in RPKM, and normalized VDJ read burden were determined via RNA
398 sequencing as previously described and were subsequently included as covariates in the
399 model.[3,22,23] For each comparison, a separate, paired design matrix that accounts for methylation
400 status in the counts matrix was used. Differential methylation was assessed using a likelihood
401 ratio test via the edgeR package.

402

403 *Global DM signatures*

404 Differential methylation signatures using all pooled tumor and adjacent samples over all patients
405 were computed with generalized linear models using edgeR's RRBS pipeline. The design matrix
406 accounted for HBV viral expression and normalized VDJ read burden determined as previously
407 described, and multiple samples from the same patient. Differential methylation along three major
408 axes were assessed with a likelihood ratio test: normal vs tumor, VDJ read burden, and HBV viral
409 expression.

410

411 <u>RNA-seq differential expression analysis and integration with DM promoters</u>

412 To compare expression-based ITH with DM promoter-based mITH, matched RNA sequencing for
413 the MSSM cohort was obtained and processed as previously described.[3] To ensure a fair
414 comparison between the RNAseq and the RRBS, generalized linear models for DE analysis were
415 generated using the edgeR pipeline with using the same covariates as that used in the DM
416 analysis where reasonably applicable.[23] DE testing was performed using a likelihood ratio test in

417 edgeR for the same regional-relative and global comparisons used in DM promoter testing as
418 described above.
419
420 Enhancer analysis
421 Annotations for known enhancers were acquired from the HACER database.[24] DM Sites were
422 overlapped with the enhancer coordinates and annotated accordingly. DM directional bias in
423 enhancer-residing sites and promoter-residing sites was statistically compared using a Wilcoxon
424 test in R.
425
426 Methylation age prediction
427 Methylation based tumor age was calculated for the HCC regional samples using the CpG-site
428 based age clock described by Horvath et al.[11] As site-level coverage of the 353 CpG-sites used
429 to determine methylation age was low in the RRBS data, encompassing genes for the Horvath
430 CpG-sites were identified and beta methylation normalized values for overlapping genes from the
431 promoter-based analysis were used as proxy. Methylation age was only computed for patients
432 with regional sampling of at least one or more normal sites and two or more tumor sites (patients
433 2, 4, 8, 9, and 10), such that age predictions could be compared intratumorally and between tissue
434 types. Patient age was transformed via logit function as described previously.[11] Median computed
435 tumor and normal regional sampling ages for each patient were contrasted to calculate the patient
436 normalized relative aging factor ratio.
437
438 Survival Analysis
439 Kaplan-Meier curves and risk tables grouping patients along the median tumor methylation age
440 factor into “old” and “young” cohorts were created using the survminer R package.[25] Patients with
441 missing survival times or model feature data were removed before modeling. The log-rank test

442 was used to evaluate the difference in survival outcomes between groups, with the significance
443 and confidence intervals reported for each comparison.
444
445 Multivariate cox proportional hazard models using tumor methylation age, tumor clinical stage,
446 sex, and patient tumor mutation burden (TMB), were constructed using the 'cph' function from the
447 rms package.[26] The relative predictive power amongst survival models and to the reference model
448 was assessed by plotting prediction error curves with the pec package in R. Integrated Breier
449 scores for each model were computed with .632+ bootstrap resampling across 100 iterations
450 (B=100) and compared, with the weights of each score corresponding to the inverse likelihood of
451 being censored, with censoring times for each iteration estimated using the Kaplan-Meier
452 estimator. Brier scores for each model were compared at 75 months with significance by KS-test
453 calculated and included in the inset figure tables, corresponding to 90% of patient events.
454
455 Validation of clock-associated tumoral hyper-aging and outcome analysis in external datasets
456 Two additional Illumina 450k methylation array HCC datasets were used for validation of
457 methylation-based tumor aging and patient survival findings. To demonstrate the tumor
458 hypermethylation and regional methylation patterns seen in the main dataset, we retrieved beta-
459 normalized illumina 450k methylation array data from the GEO database project GSE83691 for
460 17 samples from multi-regionally sampled HCC liver biopsies for three patients (*HCC8010,*
461 *HCC6952*, and *HCC8257*) was retrieved.[4] These three patients were selected due to the
462 availability of matched normal data from circulating blood. Methylation based age predictions were
463 made for each sample and relative aging factor ratios between median tumor ages and normal
464 age were calculated for each patient.
465
466 To demonstrate the effects of tumor methylation age on patient survival, Illumina 450k methylation
467 array data for 377 tumor samples from the TCGA liver cancer cohort (LIHC) was retrieved from

468 the GDC portal.[17] Clinical phenotype and survival data for these patients was also retrieved. TMB
469 information was available for 366 samples, and tumor clonality was assessed using SciClone in
470 192 samples where appropriate matched mutation data was available.[27] For 188 samples where
471 matched RNA-seq data was available, the estimated VDJ read burden and TIL clonality was
472 assessed using MixCR, and logCPM expression values for PDCD1 were calculated.[28]
473 Normalized methylation beta values were calculated for each site, and tumor methylation-based
474 ages were predicted using Horvath's clock. Relative tumoral age factors were calculated for each
475 patient using the ratio of the predicted tumor methylation age to the patient's age at diagnosis.
476 Patients were separated into 'old' and 'young' tumor groups based on median predicted age
477 factor, and survival analyses were carried out as described above. Tumor clonality, VDJ burden,
478 TMB, and PDCD1 expression was statistically compared between tumor groups using a Wilcoxon
479 rank-sum test in R.

480 **DATA AND CODE AVAILABILITY**

481 RNA sequencing data is deposited in ArrayExpress under the accession E-MTAB-5905.
482 Reduced-representation sequencing data is deposited in SRA under the accession
483 PRJNA662974. Sequencing data from patient 5 are not deposited due to lack of patient-specific
484 deposition consent. TCGA-LIHC data were generated and made available by the TCGA Research
485 Network (https://www.cancer.gov/tcga) and were downloaded from the National Cancer Institute's
486 GDC Data Portal (https://portal.gdc.cancer.gov/). Data and code will be available on GitHub upon
487 publication.

488

489 **ETHICS STATEMENT**

490 All tumor samples used in this study were collected from consented patients enrolled in the Icahn
491 School of Medicine at Mount Sinai institutional IRB-approved cancer biorepository tissue
492 procurement protocol.

493

494 **FUNDING**

495 This work was funded by the Genetics and Genomics department, Icahn School of Medicine at
496 Mount Sinai, as well as the Icahn Institute for Data Science and Genomic Technology. AV is
497 supported by the NIH (1U01CA283931-01)

498

499 **AUTHOR CONTRIBUTIONS**

500 B.L. and A.V. conceived the study concept and experimental design. PR and AB analyzed the
501 data under supervision from BL. PR, AB, DCC, BL, and AV wrote the manuscript. A.J.C collected
502 and prepared samples for RRBS sequencing.

503 **ACKNOWLEDGEMENTS**

504 The authors thank the office of Scientific Computing and the Genomics Core Facility at the Icahn
505 School of Medicine at Mount Sinai (ISMMS) for providing computational resources and staff
506 expertise, as well as the ISMMS Tisch Cancer Institute Biorepository for providing the samples.

507

508 **DISCLOSURES**

509 AV has received consulting fees from FirstWorld, Pioneering Medicine and Genentech; advisory
510 board fees from BMS, Roche, Astra Zeneca, Eisai, and NGM Pharmaceuticals; and research
511 support from Eisai. He has stock options from Espervita and Atzeyo. He is listed as an inventor
512 on a patent related to early detection of HCC (PCT/US20/61441).

513 **REFERENCES**

514 1. Bray, F., et al., *Global cancer statistics 2018: GLOBOCAN estimates of incidence and*
515 *mortality worldwide for 36 cancers in 185 countries.* CA Cancer J Clin, 2018. **68**(6): p. 394-
516 424.
517 2. Villanueva, A., *Hepatocellular Carcinoma.* N Engl J Med, 2019. **380**(15): p. 1450-1462.
518 3. Losic, B., et al., *Intratumoral heterogeneity and clonal evolution in liver cancer.* Nat
519 Commun, 2020. **11**(1): p. 291.
520 4. Lin, D.C., et al., *Genomic and Epigenomic Heterogeneity of Hepatocellular Carcinoma.*
521 Cancer Res, 2017. **77**(9): p. 2255-2265.
522 5. Zhai, W., et al., *The spatial organization of intra-tumour heterogeneity and evolutionary*
523 *trajectories of metastases in hepatocellular carcinoma.* Nat Commun, 2017. **8**: p. 4565.
524 6. Craig, A.J., et al., *Tumour evolution in hepatocellular carcinoma.* Nat Rev Gastroenterol
525 Hepatol, 2020. **17**(3): p. 139-152.
526 7. Friemel, J., et al., *Intratumor heterogeneity in hepatocellular carcinoma.* Clin Cancer Res,
527 2015. **21**(8): p. 1951-61.
528 8. Ding, X., et al., *Genomic and Epigenomic Features of Primary and Recurrent*
529 *Hepatocellular Carcinomas.* Gastroenterology, 2019. **157**(6): p. 1630-1645 e6.
530 9. Villanueva, A., et al., *DNA methylation-based prognosis and epidrivers in hepatocellular*
531 *carcinoma.* Hepatology, 2015. **61**(6): p. 1945-56.
532 10. Tischoff, I. and A. Tannapfe, *DNA methylation in hepatocellular carcinoma.* World J
533 Gastroenterol, 2008. **14**(11): p. 1741-8.
534 11. Horvath, S., *DNA methylation age of human tissues and cell types.* Genome Biol, 2013.
535 **14**(10): p. R115.
536 12. Horvath, S. and K. Raj, *DNA methylation-based biomarkers and the epigenetic clock*
537 *theory of ageing.* Nat Rev Genet, 2018. **19**(6): p. 371-384.
538 13. Zhu, T., et al., *CancerClock: A DNA Methylation Age Predictor to Identify and Characterize*
539 *Aging Clock in Pan-Cancer.* Front Bioeng Biotechnol, 2019. **7**: p. 388.
540 14. Garrett-Bakelman, F.E., et al., *Enhanced reduced representation bisulfite sequencing for*
541 *assessment of DNA methylation at base pair resolution.* J Vis Exp, 2015(96): p. e52246.
542 15. Cho, J.W., et al., *The importance of enhancer methylation for epigenetic regulation of*
543 *tumorigenesis in squamous lung cancer.* Exp Mol Med, 2022. **54**(1): p. 12-22.
544 16. Xiong, L., et al., *Aberrant enhancer hypomethylation contributes to hepatic carcinogenesis*
545 *through global transcriptional reprogramming.* Nat Commun, 2019. **10**(1): p. 335.
546 17. Cancer Genome Atlas Research Network. Electronic address, w.b.e. and N. Cancer
547 Genome Atlas Research, *Comprehensive and Integrative Genomic Characterization of*
548 *Hepatocellular Carcinoma.* Cell, 2017. **169**(7): p. 1327-1341 e23.
549 18. Bell, C.G., et al., *DNA methylation aging clocks: challenges and recommendations.*
550 Genome Biol, 2019. **20**(1): p. 249.
551 19. Hua, X., et al., *Genetic and epigenetic intratumor heterogeneity impacts prognosis of lung*
552 *adenocarcinoma.* Nat Commun, 2020. **11**(1): p. 2459.
553 20. Gimeno-Valiente, F., et al., *DNA methylation cooperates with genomic alterations during*
554 *non-small cell lung cancer evolution.* Nat Genet, 2025. **57**(9): p. 2226-2237.
555 21. European Association For The Study Of The, L., R. European Organisation For, and C.
556 Treatment Of, *EASL-EORTC clinical practice guidelines: management of hepatocellular*
557 *carcinoma.* J Hepatol, 2012. **56**(4): p. 908-43.
558 22. Chen, Y., et al., *Differential methylation analysis of reduced representation bisulfite*
559 *sequencing experiments using edgeR.* F1000Res, 2017. **6**: p. 2055.
560 23. Robinson, M.D., D.J. McCarthy, and G.K. Smyth, *edgeR: a Bioconductor package for*
561 *differential expression analysis of digital gene expression data.* Bioinformatics, 2010.
562 **26**(1): p. 139-40.

24. Wang, J., et al., *HACER: an atlas of human active enhancers to interpret regulatory variants.* Nucleic Acids Res, 2019. **47**(D1): p. D106-D112.
25. Kassambara, A., Kosinski, M. & Biecek, P., *survminer: Drawing Survival Curves using 'ggplot2'*. 2020.
26. Harrell, F.E., *rms: Regression Modeling Strategies*. 2020.
27. Miller, C.A., et al., *SciClone: inferring clonal architecture and tracking the spatial and temporal patterns of tumor evolution.* PLoS Comput Biol, 2014. **10**(8): p. e1003665.
28. Bolotin, D.A., et al., *MiXCR: software for comprehensive adaptive immunity profiling.* Nat Methods, 2015. **12**(5): p. 380-1.

FIGURES

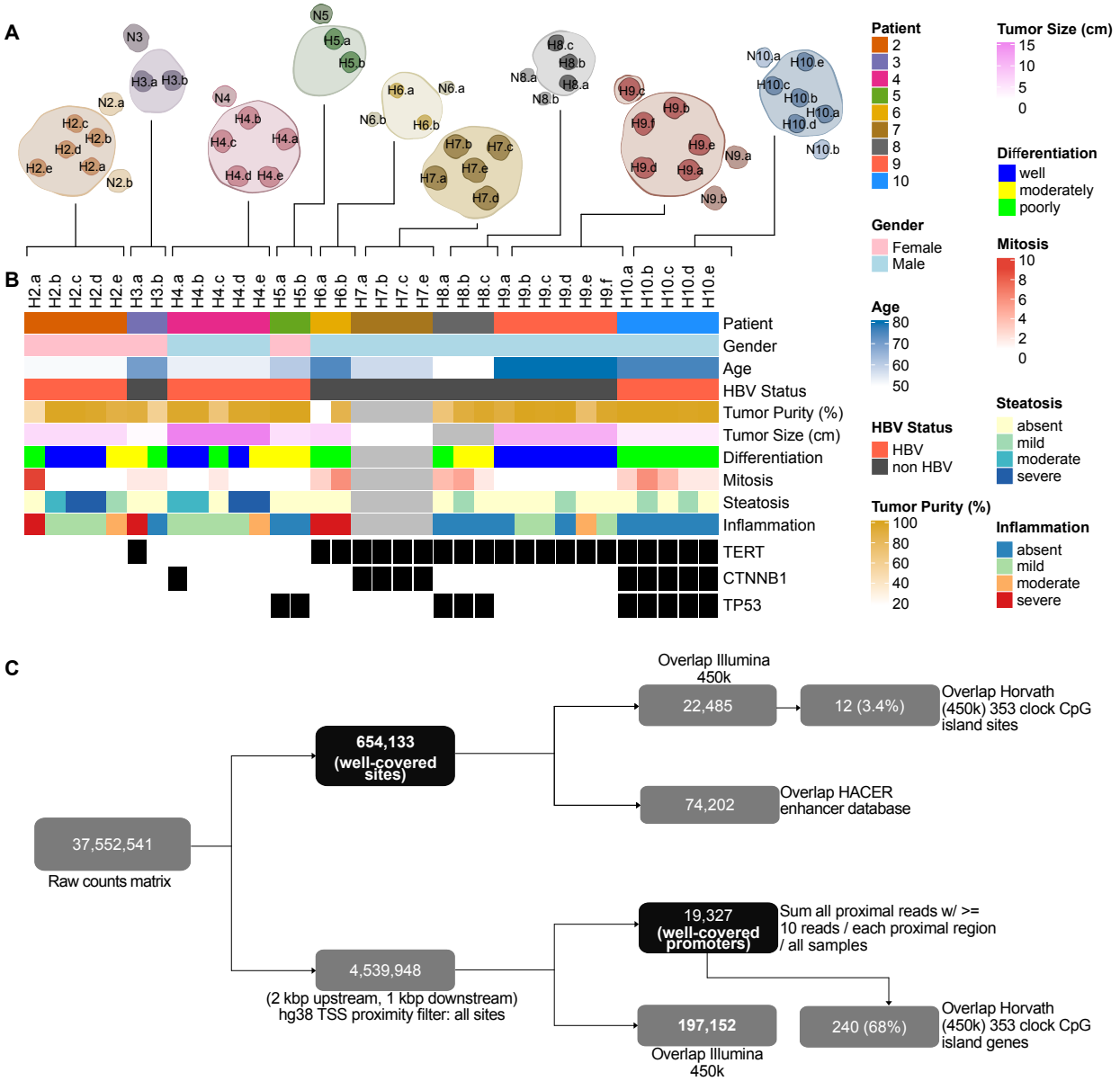

Figure 1. Study cohort and RBBS analysis workflow A) Representation of multi-regional sampling for tumors used in this study, and available data types used. B) Heatmap showing clinical features of samples, including TERT, CTNNB1, and TP53 mutation status. C) Flow chart indicating RRBS processing and analysis framework.

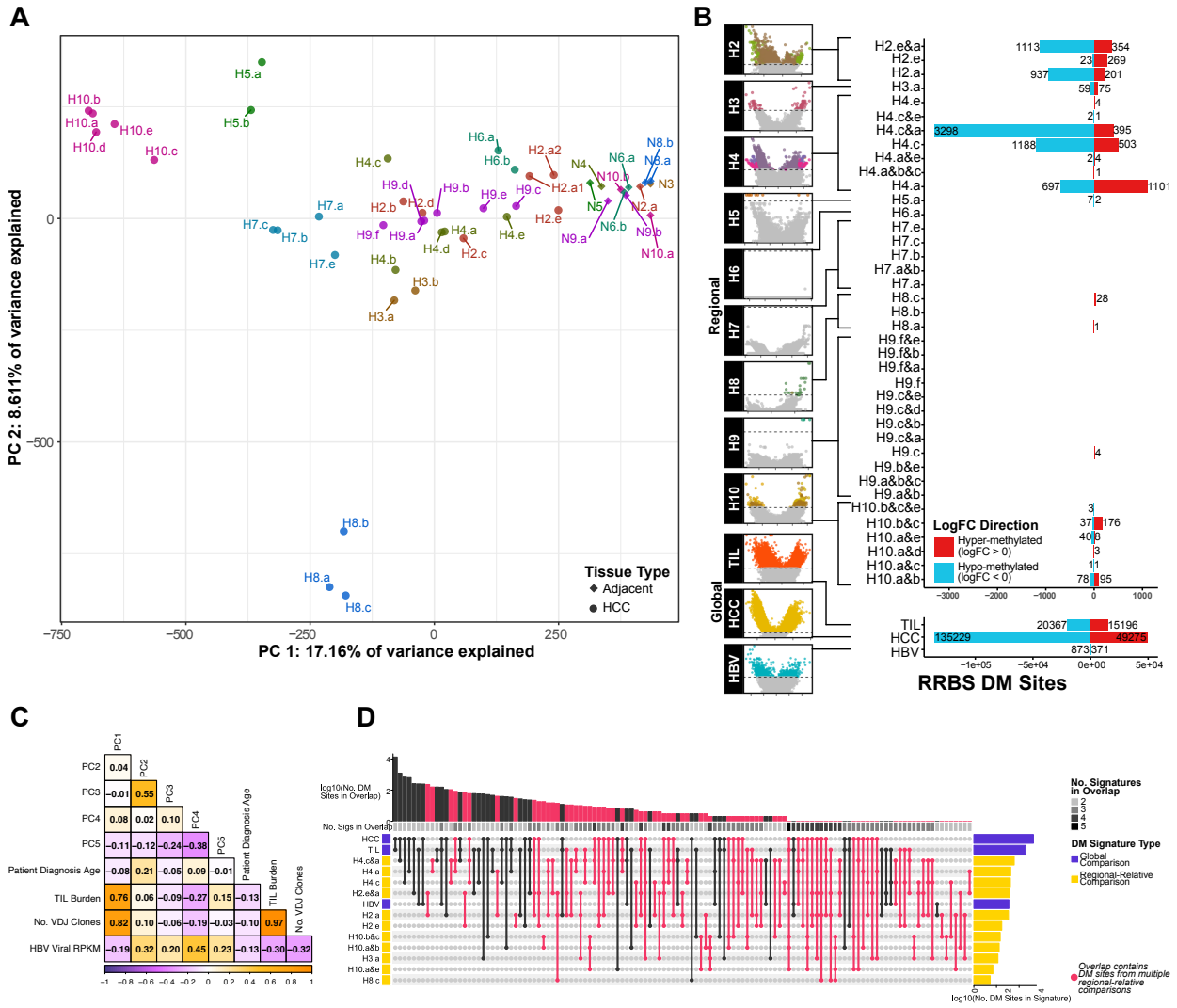

Figure 2. Differentially methylated sites. A) PCA of beta values. B) DM Sites in regional-relative and global comparisons. C) Correlation heatmap of MSSM cohort sample clinical, phenotype, and PCA. D) UpSet plot comparing shared significant DM sites across intra-patient, inter-patient, and global comparisons.

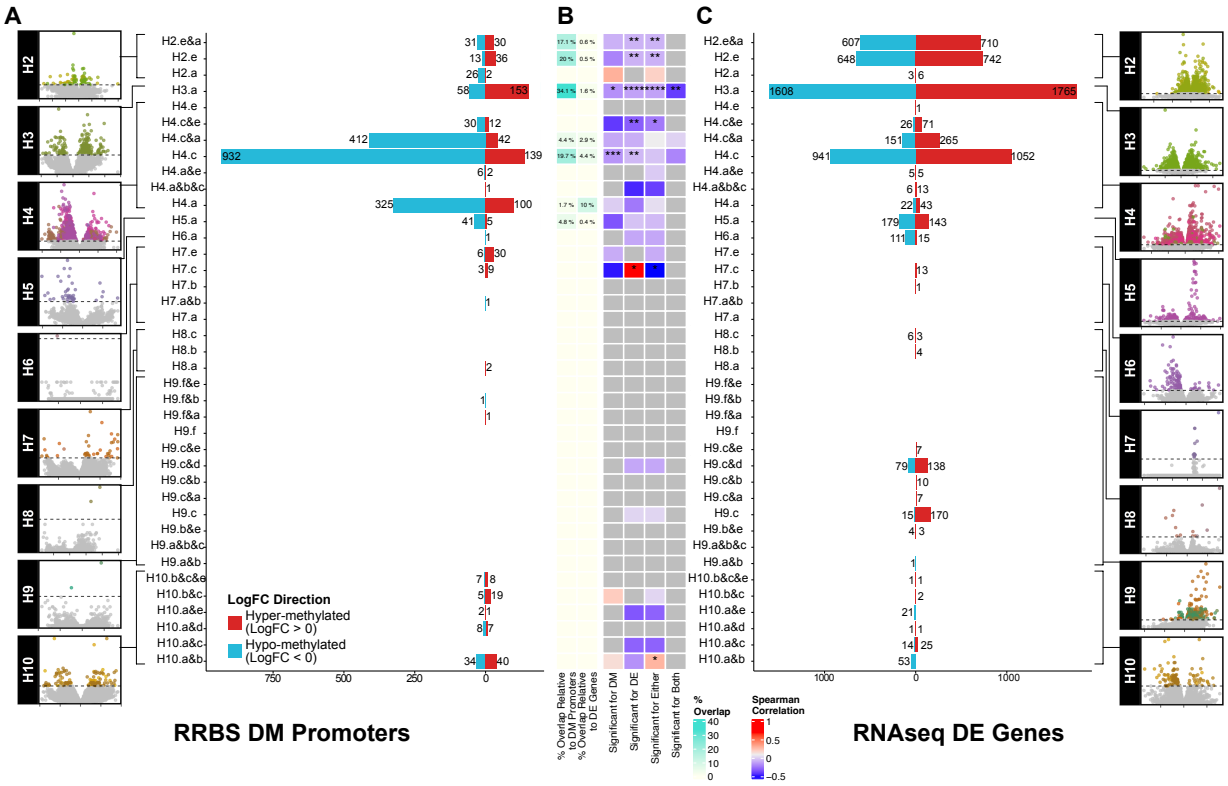

Figure 3. Regional analysis of differential methylation and expression A) Regional-relative DM promoter profiling. B) Overlap between significant DM promoters from RRBS promoter regions and significant DE genes in matched RNA seq. C) Regional DE gene profiling via RNA-seq.

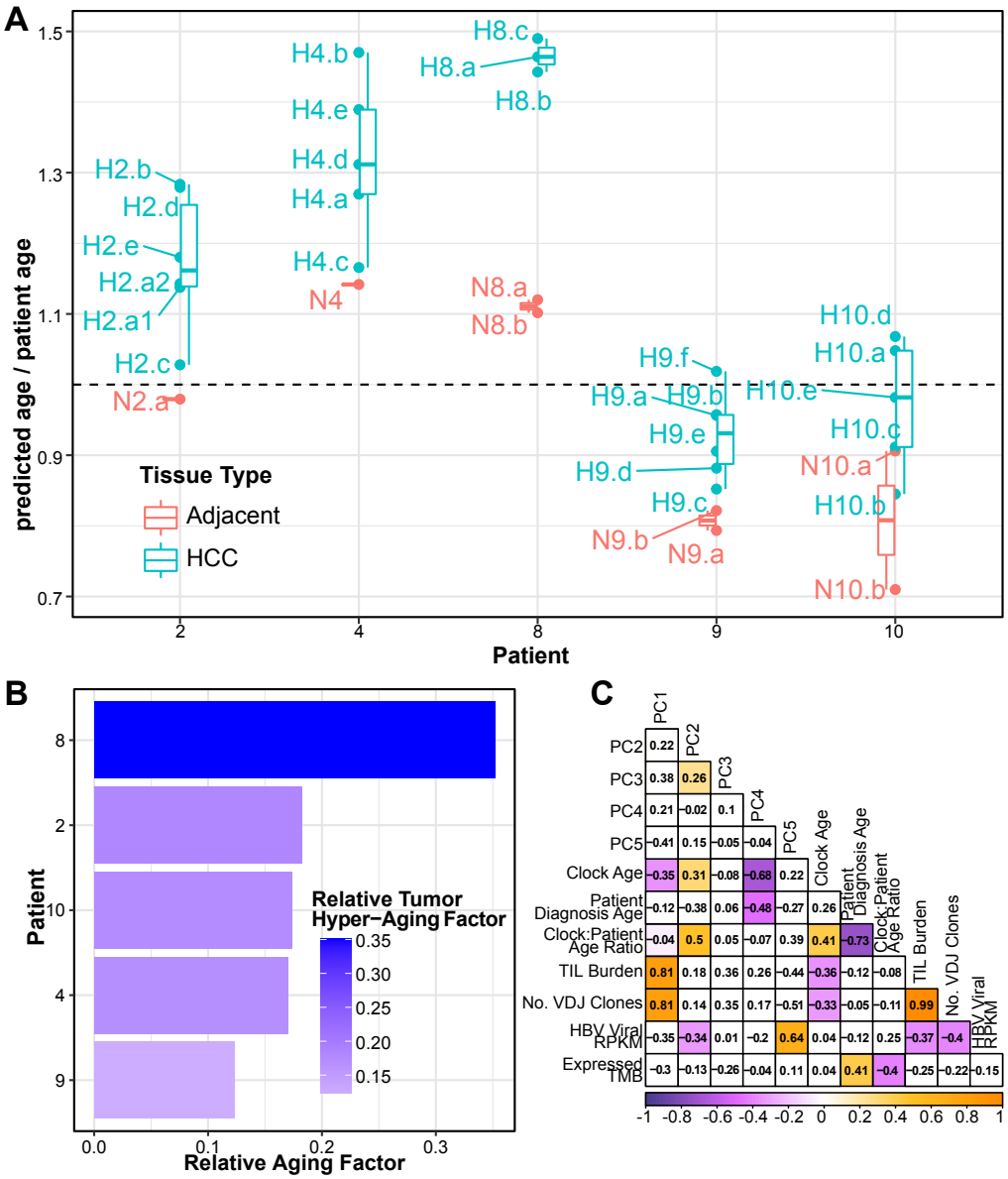

Figure 4. Tumor methylation aging relative to patient age A) Ratio of predicted tumor methylation age to patient age across regionally sampled patients. B) Hyper-aging relative to tumor methylation age in adjacent normal explains patient 8 outlier status through accelerated tumoral hyper-aging. C) Correlation heatmap of MSSM cohort sample clinical, phenotype, and PCA with methylation clock age and relative age factors across promoter-aggregated regions.

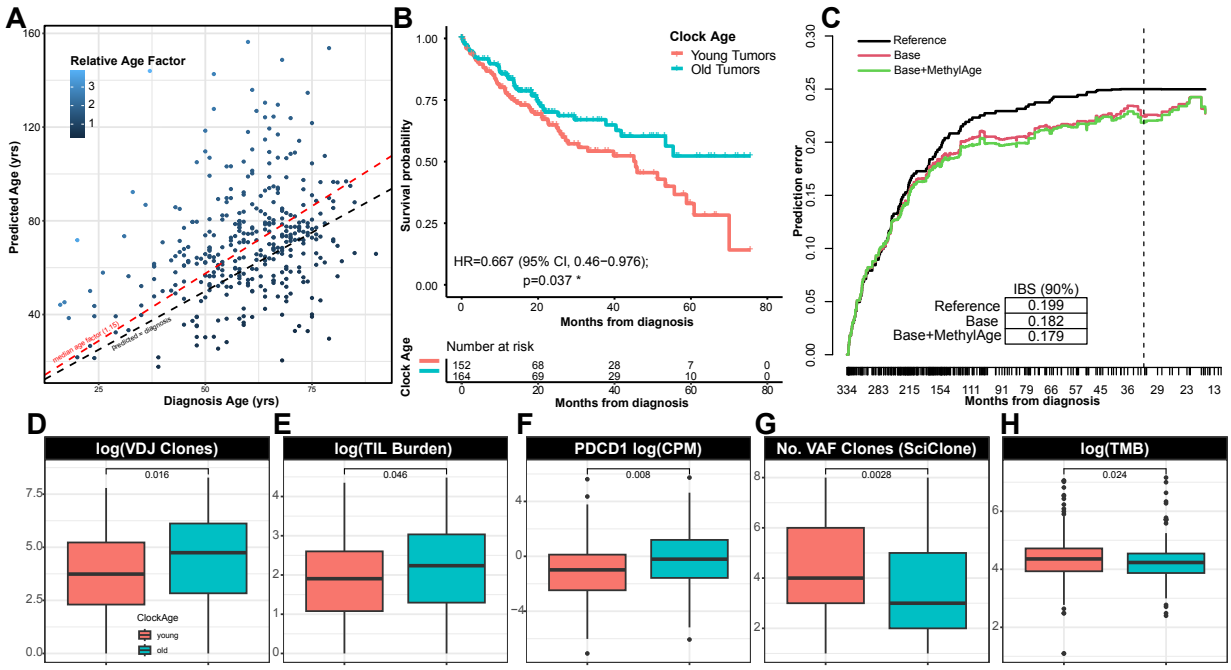

Figure 5. TCGA validation of tumor-methylation age and hyper-aging A) Age factor landscape of HCC tumors from TCGA LIHC. B) Kaplan-Meier analysis illustrates the survival benefit of “old” tumors with relative hyper-aging signature. C) Comparison of prediction error across cph models. A survival model including the predicted methylation age factor outperforms the model using only covariates of clinical tumor stage, sex, and TMB, across 90% of patient events. D) LIHC HCC relative methylation age factor tracks with known clinical markers including VDJ clone count, E) TIL burden, F) PD-1 expression from RNA-seq G) number of tumor subclones estimated via SciClone, and H) tumor mutation burden (total number of somatic mutations).

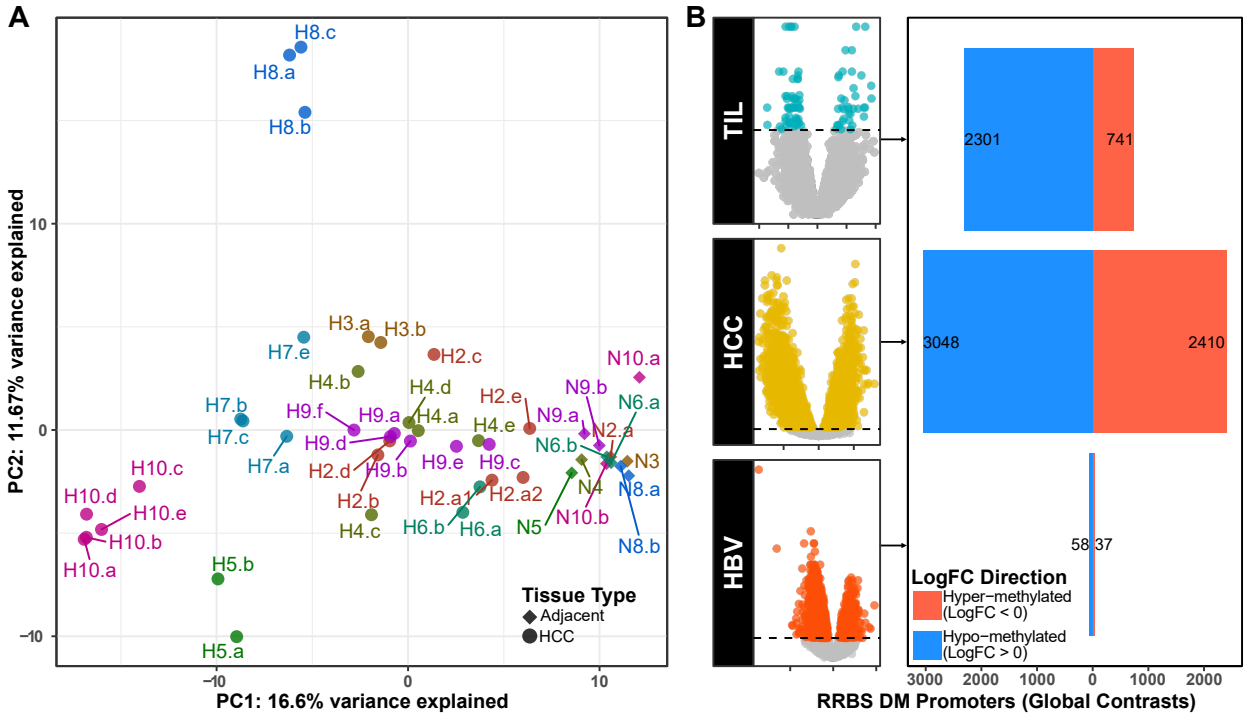

606

607 **Supplementary Figure 1. Regional promoter methylation and global promoter contrasts** A)

608 PCA of promoter aggregated methylation beta matrix. B) RRBS DM promoters for global contrasts

609 of (top to bottom) TIL, Tumor vs Adjacent, and HBV.

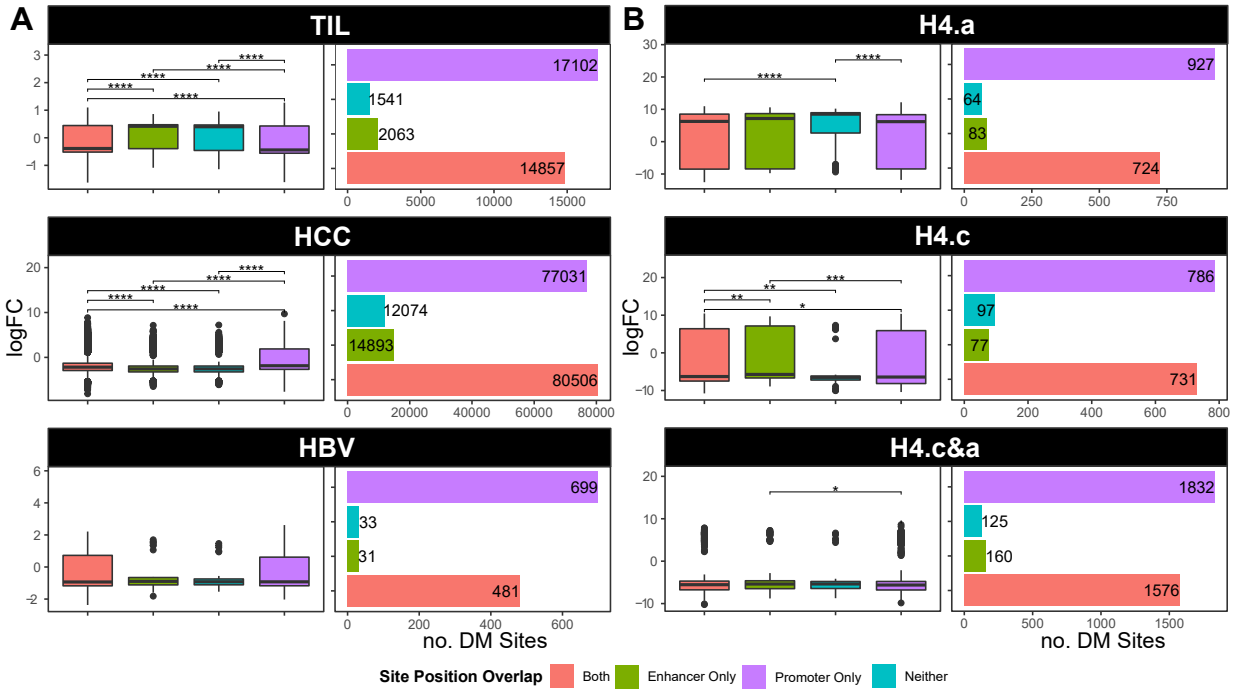

610

611 **Supplementary Figure 2. Methylation change comparisons across DM regions** covering

612 promoter, enhancer, both, or neither feature loci for A) global contrasts (top to bottom) TIL, Tumor

613 vs Adjacent, and HBV; B) regional contrasts across HCC in patient 4.

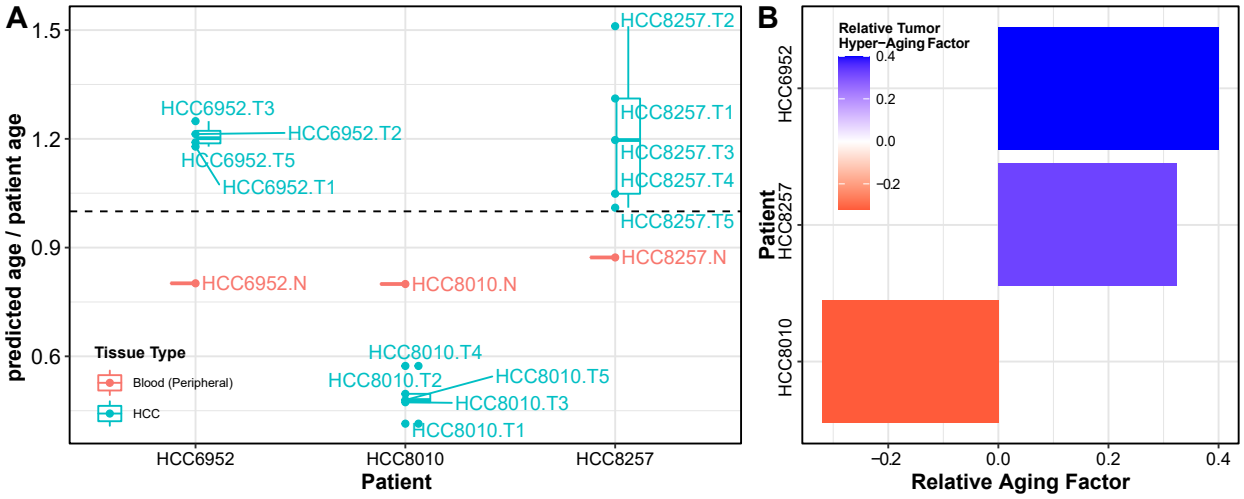

614

615 **Supplementary Figure 3. Tumoral hyper-aging validation via GSE83691.**[4] A) Site-by-site

616 methylation predicted age to patient age ratios across three multi-regionally sampled HCCs. B)

617 Tumoral methylation hyper-aging observed in two tumors, and one with hypo-aged tumor.